Radiopharmaceuticals Hot Paper

How to cite: *Angew. Chem. Int. Ed.* **2022,** *61,* e202207120
International Edition: doi.org/10.1002/anie.202207120
German Edition: doi.org/10.1002/ange.202207120

Boosting Bismuth(III) Complexation for Targeted α-Therapy (TAT) Applications with the Mesocyclic Chelating Agent AAZTA**

Dávid Horváth, Adrienn Vágner, Dezsö Szikra, György Trencsényi, Nicola Demitri, Nicol Guidolin, Alessandro Maiocchi, Simona Ghiani, Fabio Travagin, Giovanni B. Giovenzana, and Zsolt Baranyai**

Dedicated to Dr. Pier Lucio Anelli on the occasion of his retirement

Abstract: Targeted α therapy (TAT) is a promising tool in the therapy of cancer. The radionuclide $^{213}Bi^{III}$ shows favourable physical properties for this application, but the fast and stable chelation of this metal ion remains challenging. Herein, we demonstrate that the mesocyclic chelator AAZTA quickly coordinates Bi^{III} at room temperature, leading to a robust complex. A comprehensive study of the structural, thermodynamic and kinetic properties of $[Bi(AAZTA)]^-$ is reported, along with bifunctional $[Bi(AAZTA\text{-}C4\text{-}COO^-)]^{2-}$ and the targeted agent $[Bi(AAZTA\text{-}C4\text{-}TATE)]^-$, which incorporates the SSR agonist Tyr^3-octreotate. An unexpected increase in the stability and kinetic inertness of the metal chelate was observed for the bifunctional derivative and was maintained for the peptide conjugate. A cyclotron-produced $^{205/206}Bi$ mixture was used as a model of ^{213}Bi in labelling, stability, and biodistribution experiments, allowing the efficiency of $[^{213}Bi(AAZTA\text{-}C4\text{-}TATE)]^-$ to be estimated. High accumulation in AR42J tumours and reduced kidney uptake were observed with respect to the macrocyclic chelate $[^{213}Bi(DOTA\text{-}TATE)]^-$.

Introduction

Targeted α therapy (TAT) is currently being actively investigated as a potential treatment of cancer relying on α-emitting radionuclides. α-particles can transfer high linear energy in a short range, allowing an internal radiotherapy confined in a limited area while reducing off-target damage. Among α-emitting radionuclides, ^{213}Bi ($t_{1/2}=46$ min) deserves a special mention since its availability through commercially available benchtop generators and its usefulness in the preparation of agents for TAT. Clinical trials have been undertaken with ^{213}Bi-based TAT agents, with the radionuclide covalently bound to antibodies or to small peptides (octreotide and analogues), the latter showing promising results for neuroendocrine tumours and gliomas.[1–3] Moreover, thanks to its concomitant γ-emission, ^{213}Bi can be used as radiotracer in SPECT imaging, too.[4]

Radionuclides in TAT agents are generally in the form of metal chelates, with the chelating agents bearing an additional functional group (bifunctional chelating agents, BFCAs) for the covalent link to the targeting (bio)molecule. The chelating agent must form thermodynamically and kinetically stable complexes with the α-emitter metal ion. On the other hand, the limited half-lives of most isotopes relevant to TAT claim for a rapid and efficient formation of the metal complex, implying a fast complexation kinetics.[5,6]

Different chelating agents (CAs) have been scrutinised for an efficient complexation of Bi^{III} (isotopes) (Figure 1).

[*] D. Horváth
Department of Physical Chemistry, University of Debrecen
Egyetem tér 1, 4010 Debrecen (Hungary)
Dr. A. Vágner, Dr. D. Szikra, Dr. G. Trencsényi
Scanomed Ltd.
Nagyerdei Krt. 98, 4032 Debrecen (Hungary)
Dr. D. Szikra, Dr. G. Trencsényi
Medical Imaging Clinic, University of Debrecen
Nagyerdei krt. 98, 4032 Debrecen (Hungary)
Dr. N. Demitri
Elettra-Sincrotrone Trieste
S.S. 14 Km 163.5 in Area Science Park, 34149 Basovizza (TS) (Italy)
N. Guidolin, Dr. A. Maiocchi, Dr. S. Ghiani, Dr. Z. Baranyai
Bracco Imaging Spa, Bracco Research Centre
Via Ribes 5, 10010 Colleretto Giacosa (TO) (Italy)
E-mail: zsolt.baranyai@bracco.com
Dr. F. Travagin, Prof. G. B. Giovenzana
Dipartimento di Scienze del Farmaco, Università del Piemonte Orientale
Largo Donegani 2/3, 28100 Novara (Italy)
E-mail: giovanni.giovenzana@uniupo.it

[**] **AAZTA** = 1,4-bis(carboxymethyl)-6-[bis(carboxymethyl)]amino-6-methylperhydro-1,4-diazepine

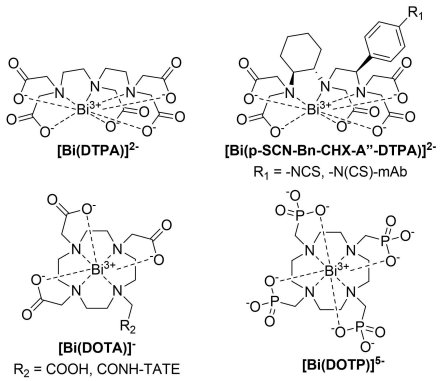

Figure 1. Bi^{III}-complexes for biomedical applications.

Acyclic CAs as DTPA form Bi^{III}-complexes with modest inertness, generally not suitable for a safe in vivo use. Rigidification of the acyclic DTPA backbone, as in CHX-DTPA, significantly improves the stability of the corresponding chelate, allowing preclinical studies.[7]

Macrocyclic CAs bind Bi^{III} with unrivalled stability and for this reason most of the investigated Bi^{III}-radiopharmaceuticals were developed starting from the "gold standard" DOTA.[8] $^{213}Bi^{III}$- and $^{225}Ac^{III}$-complexes of DOTA-peptides conjugates are currently in clinical trials as TAT-agents for the treatment of neuroendocrine tumours.[2,8] De Swart et al. demonstrated that $[^{213}Bi(DOTA\text{-}TATE)]^-$ can be used as radiotracer for SPECT imaging, broadening the scope of $^{213}Bi^{III}$-complexes from therapy to diagnosis, and to theranostics.[4] However the formation of Bi^{III}-complexes with DOTA is quite slow and requires high temperatures for long reaction times and high concentration of ligand (30–60 min at 95 °C, pH 4–9, [DOTA] = 10 μM)[8] to complete. These conditions are hardly compatible with the preparation of labile bioconjugates and detrimental in terms of residual radio-activity, taking a time comparable to one half-life of ^{213}Bi.[9,10]

The variation of the pendant arms of the macrocyclic CAs was demonstrated to be a possible strategy to speed up the formation kinetics of Bi^{III}-complexes.[11] The phosphonate analogue DOTP was recently shown to combine a higher thermodynamic stability with a faster complexation kinetics with respect to the carboxylic counterpart.[9,12] Other related CAs bearing phosphonate and phosphinate groups displayed an analogous increased rate of Bi^{III}-complexation,[13] paving the way for bone cancer treatment by taking advantage of the tropism for bone tissue provided by the phosphonate groups.[14]

The coordination chemistry of Bi^{III} with polyaminocarboxylic CAs is scarcely investigated, and no systematic investigation has been reported on the complexation of this metal ion with mesocyclic chelating agents. Among them, 6-amino-6-methylperhydro-1,4-diazepinetetraacetic acid (AAZTA)[15] proved to be an efficient coordinating system for several metal ions in the lanthanoids, transition and post-transition metals.[16,17] Thanks to its simply editable structure, it lends itself to many modifications with the aim of tuning its chelating properties[18–20] and of preparing bifunctional derivatives for conjugation purposes.[21]

BFCAs derived from the parent AAZTA (Figure 2) include AAZTA-C4 and AAZTA-C9, both used as starting point for the preparation of targeted agents for nuclear medicine applications. AAZTA-C9-minigastrin has been efficiently radiolabelled with ^{68}Ga, ^{177}Lu and ^{111}In, selectively targeting CCDK2+ tumour cells and has been successfully exploited in murine models of gastrointestinal cancers.[22] Similarly, AAZTA-C4-TOC has been rapidly and quantitatively radiolabelled with $^{68}Ga^{III}$, $^{44}Sc^{III}$ and $^{177}Lu^{III}$ at room temperature and studied in the detection and treatment of neuroendocrine tumours.[6] Finally, AAZTA-C4 has been bioconjugated through a squaric acid linker to PSMA-617, and radiolabelled with $^{44}Sc^{III}$, $^{64}Cu^{II}$, $^{68}Ga^{III}$ and $^{177}Lu^{III}$, with the aim of delivering radionuclides to prostate cancer.[23,24]

In general, the mesocyclic AAZTA-based systems quickly and quantitatively form stable chelates at or close to room temperature. These mild conditions are particularly valuable for the preparation of radiobioconjugates with short-lived isotopes, limiting the degradation of the (bio)molecules and ensuring the maximum and correct dosage to the patient.[6]

Prompted by these results, we investigated the potential application of AAZTA as a platform for the development of Bi^{III}-based TAT agents, as the mesocyclic AAZTA structure can easily satisfy the large coordination sphere of this distinctive metal ion.

Moreover, the mesocyclic chelating platform has been exploited for the preparation of the targeted agent $[Bi(AAZTA\text{-}C4\text{-}TATE)]^-$, embodying the SSR agonist Tyr^3-octreotate. Herein we report a comprehensive account of the thermodynamics, formation and dissociation kinetics, solution and solid-state structural properties of the Bi^{III}-AAZTA, Bi^{III}-AAZTA-C4-COO^- and Bi^{III}-AAZTA-C4-TATE systems. Additionally, $^{205/206}Bi$-labelling of AAZTA-C4-TATE and DOTA-TATE was studied to find the best conditions for the formation of the corresponding chelates and comparing the labelling efficiency with acyclic and macrocyclic CAs. Finally, the in vivo efficiency and biodistribution of $[^{205/206}Bi(AAZTA\text{-}C4\text{-}TATE)]^-$ complex were also investigated in animal model.

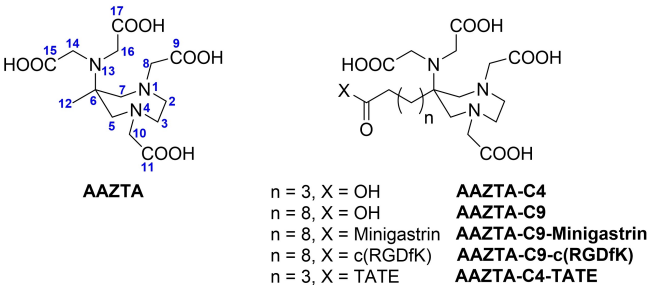

Figure 2. AAZTA, bifunctional derivatives and conjugates.

Results and Discussion

Synthesis of AAZTA-C4-TATE

The linear octapeptide H-D-Phe-Cys(Acm)-Tyr(*t*Bu)-*D*-Trp(Boc)-Lys(Boc)-Thr(*t*Bu)-Cys(Acm)-Thr(*t*Bu), precursor of octreotate, protected, oxidised and linked to the Wang resin (**1**) was prepared in an automatic peptide synthesiser by standard Fmoc protocol as reported by Petersen et al.[25,26] AAZTA-C4-(*t*-Bu)$_4$ was prepared as described by Manzoni et al.[27] AAZTA-C4 was conjugated to the N-terminus of the protected octapeptide by treatment with HATU/collidine in DMF in a SPPS manual reactor in 3 h at room temperature. After the coupling, the resin was washed with DMF and the conjugate was cleaved from the resin and fully deprotected by treatment with TFA/H_2O/triisopropylsilane in 18 h at room temperature. AAZTA-C4-TATE (Figure 3) was purified by preparative HPLC.

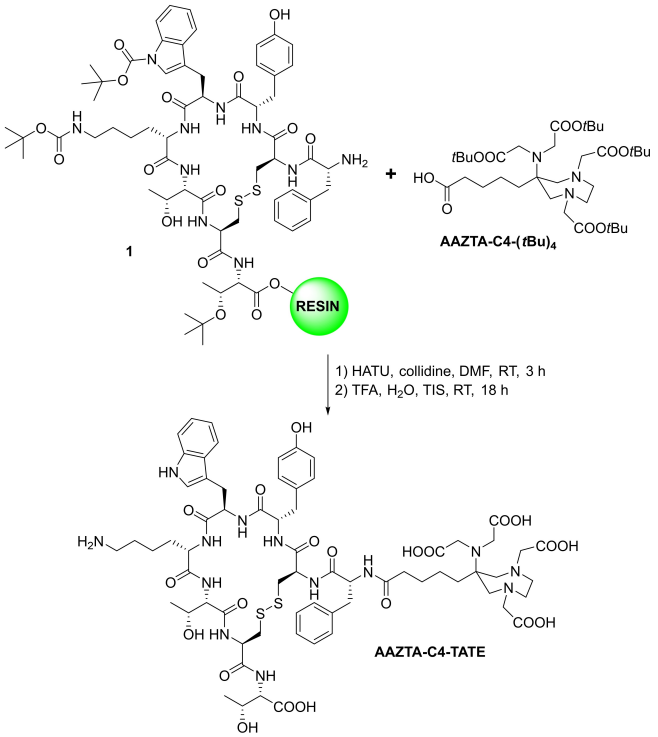

Figure 3. Preparation of AAZTA-C4-TATE.

Thermodynamic and Kinetic Properties of [Bi(AAZTA)]$^-$, [Bi(AAZTA-C4-COO$^-$)]$^{2-}$ and [Bi(AAZTA-C4-TATE)]$^-$

Two key parameters for safe and efficient in vivo applications of metal complexes are the thermodynamic stability and kinetic inertness or kinetic stability, required to avoid the release of the metal ion and of the free ligand and the delivery of the radioisotope as intact complex to the target organ or tissue. Despite the high thermodynamic stability constant, the extremely low concentration of the radiopharmaceuticals and the high excess of the possible endogenous competitors (transmetallation and transchelation reactions) might promote the in vivo dissociation of the metal complex.[28] The stability constants of the Bi^{III}-polyaminopolycarboxylate complexes have been usually determined by spectrophotometry with the use of the competition and/or decomplexation reaction by Br^- ion[29] at acidic (pH = 2–3) or by OH^- ions[30,31] at basic conditions (pH > 11). The stability and the conditional stability constants of the [Bi(AAZTA)]$^-$, [Bi(AAZTA-C4-COO$^-$)]$^{2-}$ and [Bi(AAZTA-C4-TATE)]$^-$ complexes (Table 1) were determined by following the competition reactions between NTA and AAZTA, AAZTA-C4-COOH or AAZTA-C4-TATE ligands for Bi^{III} ion by UV spectrophotometry (Figures S3 and S4) and Capillary Zone Electrophoresis (CZE, Figure S5) in Bi^{III}—NTA-AAZTA, Bi^{III}—NTA-AAZTA-C4-COOH and Bi^{III}—NTA-AAZTA-C4-TATE systems, respectively (pH = 7.4, 25 °C, 0.15 M $NaClO_4$). Definitions and equations used for the evaluation of the thermodynamic data are reported in the Supporting Information.

The comparison of the thermodynamic parameters in Table 1 reveals that the stability constant of [Bi(AAZTA)]$^-$ is lower than that of [Bi(AAZTA-C4-COO$^-$)]$^{2-}$, [Bi(DTPA)]$^{2-}$ and [Bi(DOTA)]$^-$ complexes by about 2.5, 3 and 4 log*K* units at similar condition (0.15 M $NaClO_4$, 25 °C). In order to compare the Bi^{III} affinity of AAZTA, AAZTA-C4-COOH, AAZTA-C4-TATE, DTPA and

Table 1: Stability (logK_{BiL}), protonation (log$K_{Bi(HiL)}$) and conditional stability constants (logK_{BiL}^{cond}), dissociation rate (k_d) and half-life ($t_{1/2} = \ln 2/k_d$) values of [Bi(AAZTA)]$^-$ (A), [Bi(AAZTA-C4-COO$^-$)]$^{2-}$ (B), [Bi(AAZTA-C4-TATE)]$^-$ (C), [Bi(DTPA)]$^{2-}$ (D),[a] [Bi(DOTA)]$^-$ (E)[b] and [Bi(NTA)$_x$] (F)[b] complexes. (0.15 M $NaClO_4$, 25 °C).

	A	B	C	D	E	F
logK_{BiL}	26.45(6)	28.75(8)	–	29.29	30.86	16.97
log$K_{Bi(HL)}$	1.63(3)	**4.74(4)**	–	2.55(1)	1.38	–
logK_{BiL2}	–	–	–	–	–	9.23
logK_{BiL}^{cond} (pH = 7.4)	**23.5**	**25.6**	**24.3(2)**	**25.4**	**27.0**	**22.5**
k_d [s^{-1}]	1.3×10^{-8}	3.2×10^{-9}	–	5.3×10^{-9}	3.4×10^{-13}	–
$t_{1/2}$ [d] at pH = 7.4	**601**	**2507**	–	**1500**	$\mathbf{2.4\times10^{7}}$	–
k_d [s^{-1}]	1.7×10^{-6}	1.6×10^{-7}	1.8×10^{-7}	6.4×10^{-7}	1.3×10^{-11}	–
$t_{1/2}$ [d] at pH = 9.0	**4.8**	**50.4**	**43.4**	**12.6**	$\mathbf{6.1\times10^{5}}$	–

[a] Ref. [32] (0.6 M $NaClO_4$, 25 °C); [b] Ref. [9] (0.15 M $NaClO_4$, 25 °C).

DOTA ligands, the conditional stability of Bi^{III}-complexes ($\log K_{BiL}^{cond}$, Eq. (S5), Table 1) were calculated close to physiological conditions by taking into account the protonation constants of AAZTA, AAZTA-C4-COOH, DTPA and DOTA and the stability constants of $[Bi(AAZTA)]^-$, $[Bi(AAZTA\text{-}C4\text{-}COO^-)]^{2-}$, $[Bi(DTPA)]^{2-}$ and $[Bi(DOTA)]^-$ complexes. Surprisingly, the $\log K_{BiL}^{cond}$ values at pH = 7.4 and 25 °C indicate that the conditional stability of $[Bi(AAZTA\text{-}C4\text{-}COO^-)]^{2-}$ is higher than $[Bi(AAZTA)]^-$ and $[Bi(DTPA)]^{2-}$ by 2.1 and 0.2 log*K* units. Moreover, the improved thermodynamic property of $[Bi(AAZTA\text{-}C4\text{-}COO^-)]^{2-}$ is maintained for $[Bi(AAZTA\text{-}C4\text{-}TATE)]^-$, which has about 1 log*K* unit higher conditional stability than that of $[Bi(AAZTA)]^-$ and comparable $\log K_{BiL}^{cond}$ value with that of $[Bi(DTPA)]^{2-}$. The higher stability constant and conditional stability of $[Bi(AAZTA\text{-}C4\text{-}COO^-)]^{2-}$ and $[Bi(AAZTA\text{-}C4\text{-}TATE)]^-$ with respect to $[Bi(AAZTA)]^-$ might be explained by the higher basicity of the donor atoms ($\Sigma \log K_i^H$, Table S2) resulting in the higher affinity of AAZTA-C4-COOH and AAZTA-C4-TATE to Bi^{III}-ion. Considering the lack of the interaction between the Bi^{III}-ion and the *n*-valeric acid residue of the AAZTA-C4-COOH (protonation constants of the *n*-valeric acid residue of the AAZTA-C4-COOH free ligand ($\log K_3^H$, Table S2) and Bi^{III}-complex ($\log K_{Bi(HL)}$, Table 1) are identical), the similarity in the conditional stability of the $[Bi(AAZTA\text{-}C4\text{-}COO^-)]^{2-}$, $[Bi(AAZTA\text{-}C4\text{-}TATE)]^-$ and $[Bi(DTPA)]^{2-}$ complexes is rather surprising, by taking into account the lower denticity of AAZTA with respect to DTPA (7 *vs* 8). On the other hand, the $\log K_{BiL}^{cond}$ values in Table 1 reveal that $[Bi(DOTA)]^-$ has somewhat higher conditional stability constant, explained by the optimal size match between Bi^{III} and the coordination cage of DOTA.

The kinetic inertness of $[Bi(AAZTA)]^-$, $[Bi(AAZTA\text{-}C4\text{-}COO^-)]^{2-}$, $[Bi(DTPA)]^{2-}$ and $[Bi(AAZTA\text{-}C4\text{-}TATE)]^-$ were determined by following the transmetallation reactions by spectrophotometry and CZE in $[Bi(AAZTA)]^-$-DTPA, $[Bi(AAZTA\text{-}C4\text{-}COO^-)]^{2-}$-DOTP, $[Bi(DTPA)]^{2-}$-DOTP and $[Bi(AAZTA\text{-}C4\text{-}TATE)]^-$-AAZTA systems in the presence of excess exchanging DTPA, DOTP and AAZTA to guarantee the pseudo-first-order conditions. The kinetic data reported in Figures S7 and S9 show that the k_d values are independent of [DTPA], [DOTP] and [AAZTA] concentrations and increase with pH. This indicates that the rate-determining step of the transchelation reactions is the dissociation of the Bi^{III} complexes, followed by a fast reaction between the free Bi^{III} ion and the exchanging ligands. The dependence of the k_d values on pH can be interpreted by the formation ($K^H_{BiLH\text{-}1}$), the spontaneous ($^{dis}k_1$) and OH^- assisted dissociation ($^{dis}k_2$) of the $[Bi(L)H_{-1}]$ intermediate. Based on the X-ray structure of $[Bi(HAAZTA)(H_2O)]$ and $[Bi(AAZTA)]^-$ (see below), the Bi^{III}-ion is coordinated by 3 amino-N and 4 carboxylate-O donor atoms of AAZTA, whereas the apical coordination site is occupied by a water molecule to complete the dodecahedral coordination of the Bi^{III}-ion. X-ray structure of $[Bi(H_2DTPA)]$ reveals that the Bi^{III} ion is coordinated by 3 amino-N and 5 carboxylate-O donor atoms in a square antiprismatic geometry.[33] The formation of $[Bi(L)H_{-1}]$ intermediate might be interpreted by the substitution of the inner-sphere water molecule by the OH^- ion in $[Bi(AAZTA)(H_2O)]^-$ or by the substitution of a weakly coordinated -COO^- group by the OH- ion in $[Bi(DTPA)]^{2-}$. The $^{diss}k_1$ and $^{diss}k_2$ rate and $K^H_{BiLH\text{-}1}$ constants characterizing the formation and the dissociation of $[Bi(L)H_{-1}]$ intermediate of $[Bi(AAZTA)]^-$, $[Bi(AAZTA\text{-}C4\text{-}COO^-)]^{2-}$, $[Bi(DTPA)]^{2-}$ and $[Bi(DOTA)]^-$ complexes are shown in Table S3. The dissociation rates (k_d) and half-life values ($t_{1/2} = \ln 2/k_d$) of $[Bi(AAZTA)]^-$, $[Bi(AAZTA\text{-}C4\text{-}COO^-)]^{2-}$, $[Bi(DTPA)]^{2-}$ and $[Bi(AAZTA\text{-}C4\text{-}TATE)]^-$ complexes at pH = 7.4 and 9.0 are shown and compared with those of $[Bi(DOTA)]^-$ in Table 1. The definitions and equations used for the evaluation of the kinetic data are reported in the Supporting Information.

Comparison of the $t_{1/2}$ values in Table 1 reveals that the dissociation rate of $[Bi(AAZTA)]^-$ at pH = 7.4 and 25 °C is higher by about two and four times than that of $[Bi(DTPA)]^{2-}$ and $[Bi(AAZTA\text{-}C4\text{-}COO^-)]^{2-}$, respectively. Since the spontaneous dissociation of the $[Bi(L)H_{-1}]$ intermediate likely takes place by the simultaneous decoordination of the donor atoms, it can be assumed that the higher Bi^{III}-affinity of AAZTA-C4-COOH might result a slower dissociation of $[Bi(AAZTA\text{-}C4\text{-}COO^-)]^{2-}$ than that of $[Bi(AAZTA)]^-$ ($[Bi(AAZTA)]^-$: $\log K_{BiL} = 26.45$, $[Bi(AAZTA\text{-}C4\text{-}COO^-)]^{2-}$: $\log K_{BiL} = 28.75$, 0.15 M $NaClO_4$, 25 °C, Table 1). However, the Bi^{III}-affinity of the DTPA is similar to that of AAZTA-C4-COOH, whereas the OH^- assisted dissociation of $[Bi(DTPA)]^{2-}$ is significantly faster than that of $[Bi(AAZTA\text{-}C4\text{-}COO^-)]^{2-}$ ($[Bi(DTPA)]^{2-}$: $\log K_{BiL} = 29.29$, 0.6 M $NaClO_4$, 25 °C, Table 1). The higher kinetic inertness of $[Bi(AAZTA\text{-}C4\text{-}COO^-)]^{2-}$ might be interpreted by the higher rigidity of semi-macrocyclic AAZTA-C4-COOH ligand results in the slower dissociation of the $[Bi(AAZTA\text{-}C4\text{-}COO^-)H_{-1}]^{3-}$ intermediate than that of the $[Bi(DTPA)H_{-1}]$ formed with the flexible DTPA ligand. This hypothesis has been further supported by the 7-orders of magnitude slower spontaneous dissociation of $[Bi(DOTA)H_{-1}]$ in which Bi^{III} is tightly bound by the rigid DOTA ligand.[9] The dissociation half-life values ($t_{1/2} = \ln 2/k_d$, Table 1) of $[Bi(AAZTA\text{-}C4\text{-}TATE)]^-$, $[Bi(AAZTA\text{-}C4\text{-}COO^-)]^{2-}$, $[Bi(AAZTA)]^-$ and $[Bi(DTPA)]^{2-}$ obtained at pH = 9.0 and 25 °C indicate that the kinetic inertness of $[Bi(AAZTA\text{-}C4\text{-}TATE)]^-$ and $[Bi(AAZTA\text{-}C4\text{-}COO^-)]^{2-}$ is similar and higher by about 9 and 3.4 times than that of $[Bi(AAZTA)]^-$ and $[Bi(DTPA)]^{2-}$ complexes, respectively. The long dissociation half-life of $Bi(AAZTA\text{-}C4\text{-}TATE)]^-$ confirms that the high kinetic inertness is maintained for the peptide conjugate. By taking into account the stability and the inertness of $[Bi(AAZTA\text{-}C4\text{-}TATE)]^-$ and the half-life of $^{212/213}Bi$ isotopes (^{212}Bi: $t_{1/2} = 60$ min, ^{213}Bi: $t_{1/2} = 46$ min), $[^{212/213}Bi(AAZTA\text{-}C4\text{-}TATE)]^-$ complex is a promising candidate for targeted α-therapy.

Structural Properties of [Bi(AAZTA)]$^-$ and [Bi(AAZTA-C4-COO$^-$)]$^{2-}$

In order to acquire deeper insight into the solution structure, variable temperature (VT) multinuclear 1D and 2D NMR studies of [Bi(AAZTA)]$^-$ and [Bi(AAZTA-C4-COO$^-$)]$^{2-}$ have been performed in D_2O. VT-^{1}H and VT-^{13}C spectra of [Bi(AAZTA)]$^-$ and [Bi(AAZTA-C4-COO$^-$)]$^{2-}$ obtained in the temperature range 273–333 K are shown in Figures S11 and S12, S17 and S18, respectively. ^{1}H and ^{13}C NMR signals of [Bi(AAZTA)]$^-$ and Bi(AAZTA-C4-COO$^-$)]$^{2-}$ were assigned on the basis of COSY (Figures S13 and S19), HSQC and HMBC spectra (Figures S14, S15, S20 and S21) obtained at 273 K. Structure and the possible conformation of [Bi(AAZTA)]$^-$ and Bi(AAZTA-C4-COO$^-$)]$^{2-}$ with assignment of the ^{1}H and ^{13}C NMR signals are shown in Figures S10–S12 and S16–S18. ^{1}H- and ^{13}C NMR spectra of [Bi(AAZTA)]$^-$6ek; and Bi(AAZTA-C4-COO$^-$)]$^{2-}$ contain one single set of signals practically constant in the temperature range 273–333 K. The ^{13}C NMR spectra showed eight and twelve resonances corresponding to 2:2:2 equally intense methylene and carboxylate carbon atoms of pendant arms and the ring, and 1:1 methyl and quaternary C of [Bi(AAZTA)]$^-$ and 1:1:1:1:1:1 quaternary C, methylene and carboxylate of the *n*-valeric acid residue of Bi(AAZTA-C4-COO$^-$)]$^{2-}$ indicating that Bi^{III}-complexes has C_s symmetry in the entire temperature range. Interestingly, the ^{1}H NMR signal of the exocyclic carboxylate methylene protons in [Bi(AAZTA)]$^-$ and [Bi(AAZTA-C4-COO$^-$)]$^{2-}$ are singlet and AB system (Figures S11 and S17), revealing a higher structural rigidity of [Bi(AAZTA-C4-COO$^-$)]$^{2-}$ with respect to the parent [Bi(AAZTA)]$^-$.

It was possible to obtain single crystals of the [Bi(AAZTA)]$^-$ complex in two different protonation states, i.e.: [Bi(HAAZTA)(H_2O)]·3H_2O[34] and {[$C(NH_2)_3$][Bi(AAZTA)]}·3.5H_2O,[34] allowing a deeper insight into the structural details of this system. A simplified view of the protonated [Bi(HAAZTA)(H_2O)] and the deprotonated [Bi(AAZTA)]$^-$ complexes found in the [Bi(HAAZTA)(H_2O)]·3H_2O and {[$C(NH_2)_3$][Bi(AAZTA)]}·3.5H_2O crystals is shown in Figure 4. The bond lengths of the Bi^{III} coordination environment are given and compared with those of Sc^{III}- and Er^{III} in [Sc(AAZTA)]$^-$ and [Er(AAZTA)]$^-$ complexes in Table 2 (naming scheme in use is reported in Figure S22).

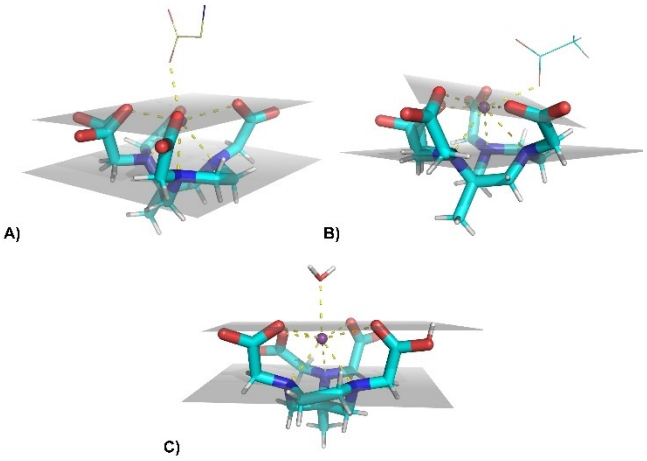

Figure 4. Stick representation of the Bi^{III} coordination environment in [Bi(AAZTA)]$^-$ (A and B) and [Bi(HAAZTA)(H_2O)] complexes found in the single crystals of [Bi(HAAZTA)(H_2O)]·3H_2O and {[$C(NH_2)_3$][Bi(AAZTA)]}·3.5H_2O.

In the single crystals of {[$C(NH_2)_3$][Bi(AAZTA)]}·3.5H_2O two crystallographically independent [Bi(AAZTA)]$^-$ complexes are placed in the asymmetric unit (Figure S22A). In both [Bi(AAZTA)]$^-$ complexes, Bi^{III} is octacoordinated by 7 donor atoms of the AAZTA chelating agent (three amino N and four carboxylate O donor atoms), whereas the eighth coordination site is occupied by a carboxylate bridging two neighbour metal centers, as previously reported for [Gd(AAZTA)]$^-$.[35] Single crystals with the formula [Bi(AAZTA)(H_2O)]}·3.H_2O show a [Bi(HAAZTA)] complex in the crystallographic asymmetric unit (Figure S22B). The [Bi(HAAZTA)] complex form dimers with units related by crystallographic inversion centers and linked by hydrogen bonds between one protonated and one deprotonated carboxylate groups ($d_{OH\cdots O}$ = 2.508(5) Å, Figure S24B). The structures of [Bi(AAZTA)]$^-$ and [Bi(HAAZTA)(H_2O)] are very similar to that of [Sc(AAZTA)(H_2O)]$^-$ and [Er(AAZTA)(H_2O)]$^-$.[36,37] The coordination polyhedrons around the Bi^{III} ion can be described by an irregular dodecahedron defined by a 1:4:3

Table 2: Bond distances (Å) in [Bi(AAZTA)]$^-$ (A and B crystallographically independent molecules, Figure 4), [Bi(HAAZTA)(H_2O)] (C, Figure 4), [Sc(AAZTA)(H_2O)]$^-$ (D) and [Er(AAZTA)(H_2O)]$^-$ (E) complexes.

	A	B	C	D[a]	E[b]
M^{3+}–OH_2	–	–	2.605(4)	2.247(1)	2.344 (9)
M^{3+}–O1	2.491(16)	2.588(16)	2.746(4)	2.202(1)	2.302 (8)
M^{3+}–O3	2.539(16)	2.723(12)	2.478(4)	2.152(1)	2.300 (8)
M^{3+}–O5	2.45(3)–2.21(5)	2.302(13)	2.439(4)	2.119(1)	2.247 (8)
M^{3+}–O7	2.606(16)	2.344(19)	2.251(4)	2.158(1)	2.290 (8)
M^{3+}–N1	2.489(17)	2.505(16)	2.587(4)	2.412(2)	2.468 (9)
M^{3+}–N2	2.592(16)	2.551(15)	2.527(4)	2.443(2)	2.569 (10)
M^{3+}–N3	2.461(18)	2.525(19)	2.486(4)	2.476(2)	2.553 (9)

[a] Ref. [36]; [b] Ref. [37]. M^{3+}–O distances of carboxylates O donor atoms bridging two Bi^{III} centers in **A**: Bi_11-O4_22 = 2.561(16) Å and in **B**: Bi_22-O4_12$1 = 2.580(14) Å.

stack (top to bottom in Figure 4) of the apical ligand (H_2O molecule in [Bi(HAAZTA)(H_2O)] or a carboxylate of the neighbor [Bi(AAZTA)]$^-$, which bridges the two metal centers, Figure 4) and of two nearly parallel pseudo-planes (7.53(10)° offset in [Bi(HAAZTA)(H_2O)] (Figure 4C) and 8.98(53)° in [Bi(AAZTA)]$^-$ (Figure 4A)): the first one involving O1, O3, O5, and O7 (mean deviation from planarity is 0.13(2) Å in [Bi(HAAZTA)(H_2O)] and 0.13(6) Å in [Bi(AAZTA)]$^-$) and the second one by N1, N2, and N3 (Figures 4A and 4 C). In Figure 4B, the Bi^{III}-ion has a slightly different coordination environment with the apical group 0.633(1) Å far from the O1, O3, O5, and O7 average plane (while is ≈2.1 Å in the other cases). The angle between the planes formed by the oxygen and nitrogen atoms remains similar (6.42(49)° – mean deviation from planarity is 0.34(25) Å; Figure 4B). In the [Sc(AAZTA)(H_2O)]$^-$ and [Er(AAZTA)(H_2O)]$^-$ complexes, the angle of the two nearly parallel planes formed by the carboxylate O and the amino N donor atoms are 8.0° and 8.3°,[36,37] which is very similar to that of [Bi(HAAZTA)(H_2O)] (Figure 4C) and [Bi(AAZTA)]$^-$ (Figure 4A). The distances between the Bi^{III} ion and the coordinated N and O atoms of AAZTA fall within the range 2.25–2.75 Å and 2.21–2.72 Å, with similar average 2.515(4) Å and 2.501(6) Å values, respectively. The average bond length of Er^{III} and Sc^{III} with the carboxylate O and amine N donor atoms of AAZTA ligand ([Er(AAZTA)]$^-$: Er^{III}–O = 2.25–2.34 Å, Er^{III}–N = 2.47–2.57 Å; [Sc(AAZTA)]$^-$: Sc^{III}–O = 2.12–2.25 Å, Sc^{III}–N = 2.41–2.47 Å) is similar to that [Bi(AAZTA)]$^-$ (Table 2). However, the distance of the water molecule from the Bi^{III} ion in [Bi(HAAZTA)(H_2O)] is significantly longer (Bi^{3+}–OH_2 = 2.605 Å, Table 2) than that of [Er(AAZTA)(H_2O)]$^-$ and [Sc(AAZTA)(H_2O)]$^-$ (Er^{3+}–OH_2 = 2.344 Å, Sc^{3+}–OH_2 = 2.247 Å, Table 2), likely explained by the "softer" character or by the stereochemical activity of the 6 s^2 lone pair of the Bi^{III}-ion.[31]

Radiolabelling of AAZTA-C4-TATE and DOTA-TATE with $^{205/206}$Bi

$^{205/206}Bi^{III}$ can be produced in cyclotron by irradiation of natural Pb- foil. Due to their easy accessibility, $^{205/206}Bi^{III}$ are ideal model isotopes for studying the radiolabelling efficiency of different ligands and the physico-chemical properties of $^{205/206}Bi^{III}$-complexes. $^{205}Bi^{III}$ (100 % β^+, $t_{1/2}$ = 15.31 d) and $^{206}Bi^{III}$ (100 % β^+, $t_{1/2}$ = 6.243 d) isotopes are produced in approximately 1:2 ratio at 16 MeV proton energy.[38] The composition of the $^{205/206}Bi^{III}$ isotope mixture constantly changes after production, complicating decay correction of the measured activity values. However, in shorter experiments, like labelling optimization and biodistribution studies (<3–4 h), the decay of the $^{205/206}Bi^{III}$ isotope can be neglected. The effect of pH, temperature and ligand concentration on the labelling of AAZTA-C4-TATE and DOTA-TATE with $^{205/206}Bi^{III}$ has been examined in detail. $^{205/206}Bi^{III}$ was purified from lead and other metal contaminants on a TK-200 resin. The labelling efficiency of AAZTA-C4-TATE and DOTA-TATE with $^{205/206}Bi^{III}$ has been examined by using 5 min reaction time at 25 and 95 °C in the presence of [AAZTA-C4-TATE] = [DOTA-TATE] = 0.1–30 μM in the pH range 3–7 (Figures 5, S26).

HEPES and ammonium-acetate as buffers were used at pH = 3 and 7 and in the pH range of 4–6, respectively. The labelling of AAZTA-C4-TATE and DOTA-TATE with $^{205/206}Bi^{III}$ was followed by thin layer chromatography (TLC) with β^+- detector. In radio-TLC, silica gel impregnated glass microfiber chromatography paper (ITLC-SG) was used with 0.5 M trisodium citrate mobile phase (pH = 5.5) which deposits the non-complexed $^{205/206}Bi^{III}$ in form of citrate complexes. The $^{205/206}Bi^{III}$-citrate complexes were eluted near the eluant front (R_f = 0.8–1) while [$^{205/206}$Bi(AAZTA-C4-TATE)]$^-$ and [$^{205/206}$Bi(DOTA-TATE)]$^-$ remained near the origin (R_f = 0.1–0.2) (Figure S27). The radiochemical yield of both $^{205/206}$Bi-complexes increases with the decrease of pH. High temperature has practically no influence on the radiochemical yield of [$^{205/206}$Bi(AAZTA-C4-TATE)]$^-$ at pH = 3, 5 and 6. However, significant increase of the radiochemical yield (RCY) values has been observed at pH = 4 and 7. High temperatures increase the radiochemical yields of [$^{205/206}$Bi(DOTA-TATE)]$^-$. The comparison of the labelling efficiency of AAZTA-C4-TATE and DOTA-TATE reveals that the incorporation of $^{205/206}$Bi by AAZTA-C4-TATE takes place with higher yields at pH = 3 and 4 (95 °C), at pH = 7 at room temperature (Figure S26). By using 5 min reaction time the optimal labelling conditions of AAZTA-C4-TATE with $^{205/206}$Bi (RCY > 95 %) was found at pH = 3, 25 °C and 95 °C in the presence of 1 μM of ligand.

The optimal labelling condition for DOTA-TATE with $^{205/206}$Bi (RCY > 95 %) was found at pH = 6 (95 °C), [DOTA-TATE] = 30 mM, 0.1 M acetate buffer, 15 min reaction time.

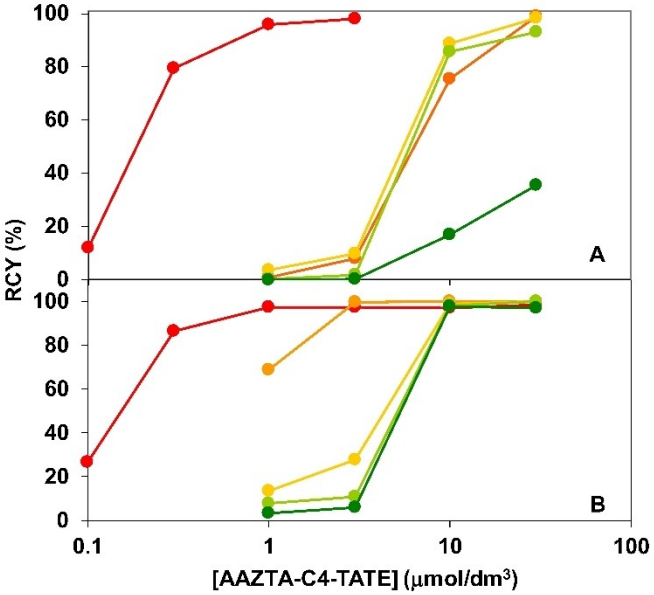

Figure 5. Labelling yield of AAZTA-C4-TATE with $^{205/206}$Bi as a function of [AAZTA-C4-TATE] at 25 °C (A) and 95 °C (B) in 5 min reaction time. (pH = 3 (●), 4 (●), 5 (●), 6 (●) and 7 (●)). Reaction volume was 100 μL and the activity of reactions was around 0.1 MBq.

The stability of [$^{205/206}$Bi(AAZTA-C4-TATE)]$^-$ has been investigated in the presence of DTPA excess, in PBS and in human plasma. For these experiments, [$^{205/206}$Bi(AAZTA-C4-TATE)]$^-$ was prepared under optimal conditions and purified by se-pack (STRATA-X). [$^{205/206}$Bi(AAZTA-C4-TATE)]$^-$ was incubated up to 21 h at pH = 7.4 and room temperature in 0.01 M DTPA solution and PBS buffer, as well as at 37 °C in human plasma (Figure 6). Constant RCP values in the examined period of time indicate the stability of [$^{205/206}$Bi(AAZTA-C4-TATE)]$^-$ in all media.

In vivo and ex vivo Distribution of [$^{205/206}$Bi(AAZTA-C4-TATE)]$^-$

The excellent results of the equilibrium, kinetic and labelling studies led to a preliminary assessment of the in vivo and ex vivo behavior of [$^{205/206}$Bi(AAZTA-C4-TATE)]$^-$. The biodistribution of [$^{205/206}$Bi(AAZTA-C4-TATE)]$^-$ has been investigated in healthy control and AR42 J tumour-bearing mice. In the ex vivo biodistribution studies AR42 J tumour-bearing SCID mice were sacrificed 15, 60 and 90 min ($n = 3$ mice/time point) after intravenous injection of [$^{205/206}$Bi-(AAZTA-C4-TATE)]$^-$ and the accumulated radioactivity of the organs and tissues were determined by gamma counter measurements after autopsy. Remarkable radiotracer accumulation was observed in kidneys (approx. %ID/g: 8–16) and urine (approx. %ID/g: 160–300) at each investigated time point, and significantly lower uptake ($p \leq 0.05$) of the radiotracer was observed in other healthy organs and tissues. The amount of the radiotracer (%ID/g) decreased continuously in each investigated organs from 15 to 90 minutes (Figure 7). The high %ID/g values (11.7 ± 1.82 at 15 min, 9.32 ± 3.96 at 60 min, and 8.53 ± 2.02 at 90 min) of the AR42 J tumour show the strong somatostatine receptor specificity of the [$^{205/206}$Bi(AAZTA-C4-TATE)]$^-$ radiotracer, which has been confirmed by the in vitro studies of the [$^{205/206}$Bi(AAZTA-C4-TATE)]$^-$ accumulation in the somatostatin receptor positive AR42 J cells (Figure S28).

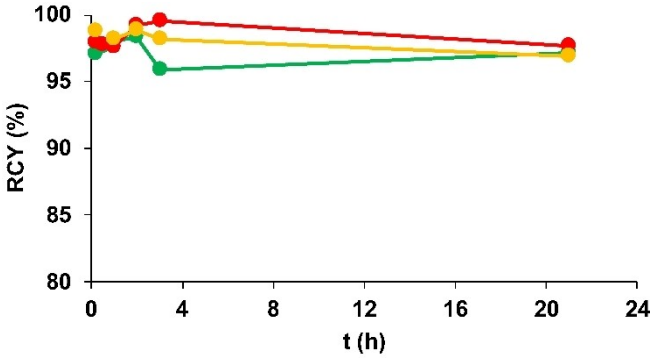

Figure 6. Stability investigation of [$^{205/206}$Bi(AAZTA-C4-TATE)]$^-$ in PBS (●) and 0.01 M DTPA (●) solutions at room temperature, and in human plasma (●) at 37 °C. The activity of the reaction mixtures was around 0.017 MBq and the reaction volume was 30 µL for DTPA and PBS stability and 100 µL for plasma stability.

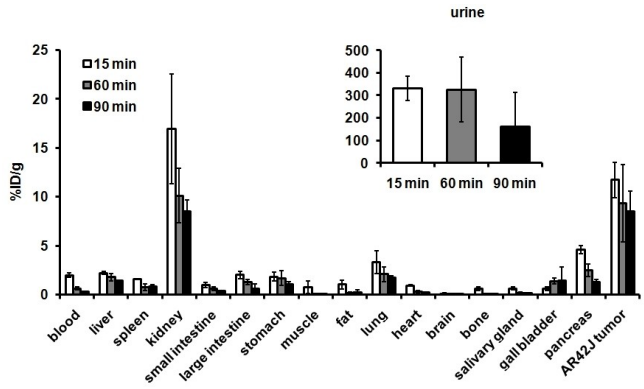

Figure 7. Ex vivo biodistribution of [$^{205/206}$Bi(AAZTA-C4-TATE]$^-$ in AR42 J somatostatine receptor positive tumour-bearing CB17 SCID mice 15, 60 and 90 min after intravenous injection of the radiotracer. %ID/g values are presented as mean ± SD.

Moreover, the ex vivo biodistribution of the free $^{205/206}$Bi^{III} radiotracer (Figure S29), which might be formed by the dissociation of the $^{205/206}$Bi^{III}-complexes, indicates high radioactivity in the liver, spleen, and kidneys, and moderate accumulation in the lungs and gall bladder after 30 and 90 min incubation time. In contrast, [$^{205/206}$Bi(AAZTA-C4-TATE)]$^-$ was only accumulated in the AR42 J tumour and kidneys due to its high stability and excretion through the urinary system (Figure 7).

In order to estimate the efficiency of [^{213}Bi(AAZTA-C4-TATE)]$^-$ as TAT agent of neuroendocrine tumours, the relative accumulated dose (%ID/g) obtained at 15, 60 and 90 min for [$^{205/206}$Bi(AAZTA-C4-TATE)]$^-$ and 10 and 60 min for [^{213}Bi(DOTA-TATE)]$^-$ in rat pancreatic AR42 J tumour-bearing athymic male nu/nu mice[39] have been compared in Table 3 (%ID/g values of [^{213}Bi(DOTA-TATE)]$^-$ were estimated for some organs based on Figure 2 in ref. [39]). Such a comparison of the biodistribution data can provide an information for in vivo behaviour of the radiotracer (i.e. efficiency) even if it was obtained with different isotopes of Bi^{III}-ion, since the decay of $^{205/206}$Bi or ^{213}Bi isotopes has practically no influence for the relative abundance of the [Bi(AAZTA-C4-TATE)]$^-$ and [Bi-(DOTA-TATE)] complexes in different organs.

The comparison of the relative biodistribution (%ID/g) of [$^{205/206}$Bi(AAZTA-C4-TATE)]$^-$ and [^{213}Bi(DOTA-TATE)]$^-$ at 60 min after the administration of the radiotracers reveals that the relative tumour uptake of [$^{205/206}$Bi-

Table 3: Accumulated dose (%ID/g) obtained at 15, 60 and 90 min for [$^{205/206}$Bi(AAZTA-C4-TATE)]$^-$ and 10 and 60 min for [^{213}Bi(DOTA-TATE)]$^-$ in tumour and other organs.

	[$^{205/206}$Bi(AAZTA-C4-TATE)]$^-$			[^{213}Bi(DOTA-TATE)]$^-$[a]	
t (min)	15	**60**	90	10	**60**
Tumour	11.7	**9.32**	8.53	5.3	**6.5**
Pancreas	4.59	**2.49**	1.27	4.0[b]	**2.5**[b]
Stomach	1.82	**1.68**	1.08	3.0[b]	**2.0**[b]
Kidney	16.7	**10.1**	8.52	18[b]	**17.4**[b]
Liver	2.19	**1.79**	1.45	n.a.	**2.0**[b]
Blood	1.98	**0.62**	0.33	9.0[b]	**1.5**[b]

[a] Ref. [39]; [b] Estimated values based on Figure 2 in Ref. [38].

(AAZTA-C4-TATE)]$^-$ is 1.5 times higher than that of [^{213}Bi(DOTA-TATE)]$^-$. The somatostatin receptor specificity of [$^{205/206}$Bi(AAZTA-C4-TATE)]$^-$ and [$^{205/206}$Bi(DOTA-TATE)]$^-$ was investigated and compared in vitro using AR42 J cell line (Figure S28). The in vitro studies indicate that the accumulation of [$^{205/206}$Bi(AAZTA-C4-TATE)]$^-$ in AR42 J cells was somewhat higher (29.76 ± 10.84 %ID/10^6 cells at 30 min; 22.99 ± 3.16 %ID/10^6 cells at 60 min) than that of [$^{205/206}$Bi(DOTA-TATE)]$^-$ (22.25 ± 3.78 %ID/10^6 cells at 30 min; 19.10 ± 6.53 %ID/10^6 cells at 60 min) after 30 and 60 min incubation time (Figure S27). The in vitro data confirms that [$^{205/206}$Bi(AAZTA-C4-TATE)]$^-$ is characterized by higher uptake towards somatostatin receptor positive cells than [$^{205/206}$Bi(DOTA-TATE)]$^-$ after 30 and 60 minutes incubation time.

On the other hand, the significantly lower %ID/g values obtained in kidneys and blood indicate a faster clearance of [$^{205/206}$Bi(AAZTA-C4-TATE)]$^-$ek; than that of [^{213}Bi-(DOTA-TATE)]$^-$. Based on the larger tumour uptake of [$^{205/206}$Bi(AAZTA-C4-TATE)]$^-$ (Table 3), the expected tumour dose of [^{213}Bi(AAZTA-C4-TATE)]$^-$ is higher than that of [^{213}Bi(DOTA-TATE)]$^-$, predicting the higher efficiency of [^{213}Bi(AAZTA-C4-TATE)]$^-$ in a TAT of neuroendocrine tumours. Moreover, the faster renal clearance of [$^{205/206}$Bi(AAZTA-C4-TATE)]$^-$ suggests a reduced kidney toxicity of [^{213}Bi(AAZTA-C4-TATE)]$^-$ compared to [^{213}Bi-(DOTA-TATE)]$^-$.

Conclusion

A comprehensive study by potentiometric, spectrophotometric, NMR and SC-XRD techniques supports the robustness of [Bi(AAZTA)]$^-$, [Bi(AAZTA-C4-COO$^-$)]$^{2-}$ and of the corresponding targeted agent [Bi(AAZTA-C4-TATE)]$^-$, embodying the SSR agonist Tyr^3-octreotate. The safety margin ensured by the thermodynamic stability and the kinetic inertness of [Bi(AAZTA)]$^-$ is unexpectedly increased in the bifunctional [Bi(AAZTA-C4-COO$^-$)]$^{2-}$ and the bioconjugate [Bi(AAZTA-C4-TATE)]$^-$. Cyclotron produced $^{205/206}$Bi mixture was used as a model of ^{213}Bi in labelling-, stability- and biodistribution experiments allowing to perform dosimetry calculations for [^{213}Bi(AAZTA-C4-TATE)]$^-$. The AAZTA-C4-TATE coordinates $^{205/206}$Bi^{III} within few minutes at room temperature, ideal conditions for a quick radiolabelling of thermolabile bioconjugated targeted agents. The in vitro stability test of [^{213}Bi(AAZTA-C4-TATE)]$^-$ reveals the constant radiochemical purity (>96 %) of the radiotracer within 21 hours at 25 °C and 37 °C in PBS, 0.01 M DTPA solution and human plasma. High accumulation in AR42 J tumour and a reduced kidney uptake of [$^{205/206}$Bi(AAZTA-C4-TATE)]$^-$ was observed with respect to the macrocyclic chelate [^{213}Bi(DOTA-TATE)]$^-$. By taking into account the high stability, kinetic inertness, fast labelling, high in vitro stability and the remarkable tumor uptake, [^{213}Bi(AAZTA-C4-TATE)]$^-$ is a promising alternative of [^{213}Bi(DOTA-TATE)]$^-$ in a TAT of neuroendocrine tumors.

In conclusion, this work demonstrated the suitability of the chelating agent AAZTA for the preparation of Bi-based radiopharmaceuticals, with clear advantages over the current gold-standard DOTA. The significantly faster formation kinetics at room temperature is ideal for the preparation of (bio)conjugated derivatives under mild experimental conditions and allows full advantage to be taken of the time window offered by ^{213}Bi, with a large safety margin ensured by the considerable kinetic inertness of the chelate.

Acknowledgements

The authors acknowledge László Balázs for the dosimetry calculations. D. H. thank the financial support for the Hungarian National Research, Development and Innovation Office (NKFIH 128201 and 134694 projects). D. H. was also supported by the Doctoral School of Chemistry at the University of Debrecen, Debrecen, Hungary. G.T. thank to Bolyai fellowship to support this work. G.B.G. and F.T. thank the financial support of grant DSF-FAR-2017 from Università del Piemonte Orientale. Open Access funding provided by Università degli Studi del Piemonte Orientale Amedeo Avogadro within the CRUI-CARE Agreement.

Conflict of Interest

ZB, AM, SG hold a patent application (WO2020099398A1) on the metal complexes reported in the article.

Data Availability Statement

The data that support the findings of this study are available in the supplementary material of this article.

Keywords: AAZTA · Bioconjugation · Bismuth · Octreotate · Targeted Alpha Therapy

[1] J. H. Turner, *Br. J. Radiol.* **2018**, *91*, 20170893–20170902.
[2] F. Bruchertseifer, A. Kellerbauer, R. Malmbeck, A. Morgenstern, *J. Labelled Compd. Radiopharm.* **2019**, *62*, 794–802.
[3] C. Kratochwil, F. L. Giesel, F. Bruchertseifer, W. Mier, C. Apostolidis, R. Boll, K. Murphy, U. Haberkorn, A. Morgenstern, *Eur. J. Nucl. Med. Mol. Imaging* **2014**, *41*, 2106–2119.
[4] J. de Swart, H. S. Chan, M. C. Goorden, A. Morgenstern, F. Bruchertseifer, F. J. Beekman, M. de Jong, M. W. Konijnenberg, *J. Nucl. Med.* **2016**, *57*, 486–492.
[5] J. Yang, Y. Kan, B. H. Ge, L. Yuan, C. Li, W. Zhao, *Acta Radiol.* **2014**, *55*, 389–398.
[6] J.-P. Sinnes, J. Nagel, F. Rösch, *EJNMMI Radiopharm. Chem.* **2019**, *4*, 18.
[7] G. Montavon, A. Le Du, J. Champion, T. Rabung, A. Morgenstern, *Dalton Trans.* **2012**, *41*, 8615–8623.
[8] S. Ahenkorah, I. Cassells, C. M. Deroose, T. Cardinaels, A. R. Burgoyne, G. Bormans, M. Ooms, F. Cleeren, *Pharmaceutica* **2021**, *13*, 599–624.
[9] D. Horváth, F. Travagin, N. Guidolin, F. Buonsanti, G. Tircsó, I. Tóth, F. Bruchertseifer, A. Morgenstern, J. Notni, G. B.

Giovenzana, Z. Baranyai, *Inorg. Chem. Front.* **2021**, *8*, 3893–3904.
[10] H. S. Chan, E. de Blois, M. Konijnenberg, A. Morgenstern, F. Bruchertseifer, W. Breeman, M. de Jong, *J. Nucl. Med.* **2014**, *55*, 1179–1179.
[11] D. J. Fiszbein, V. Brown, N. A. Thiele, J. J. Woods, L. Wharton, S. N. MacMillan, V. Radchenko, C. F. Ramogida, J. J. Wilson, *Inorg. Chem.* **2021**, *60*, 9199–9211.
[12] S. Hassfjell, K. O. Kongshaug, C. Romming, *Dalton Trans.* **2003**, 1433–1437.
[13] J. Šimeček, P. Hermann, C. Seidl, F. Bruchertseifer, A. Morgenstern, H. J. Wester, J. Notni, *EJNMMI Res.* **2018**, *8*, 78.
[14] S. P. Hassfjell, S. Bruland, P. Hoff, *Nucl. Med. Biol.* **1997**, *24*, 231–237.
[15] F. Travagin, L. Lattuada, G. B. Giovenzana, *Coord. Chem. Rev.* **2021**, *438*, 213908–213931.
[16] S. Aime, L. Calabi, C. Cavallotti, E. Gianolio, G. B. Giovenzana, P. Losi, A. Maiocchi, G. Palmisano, M. Sisti, *Inorg. Chem.* **2004**, *43*, 7588–7590.
[17] Z. Baranyai, F. Uggeri, G. B. Giovenzana, A. Bényei, E. Brücher, S. Aime, *Chem. Eur. J.* **2009**, *15*, 1696–1705.
[18] C. Guanci, G. Giovenzana, L. Lattuada, C. Platas-Iglesias, L. J. Charbonnière, *Dalton Trans.* **2015**, *44*, 7654–7661.
[19] D. Parker, B. P. Waldron, *Org. Biomol. Chem.* **2013**, *11*, 2827–2838.
[20] B. P. Waldron, D. Parker, C. Burchardt, D. S. Yufit, M. Zimny, F. Roesch, *Chem. Commun.* **2013**, *49*, 579–581.
[21] P. Minazzi, L. Lattuada, I. G. Menegotto, G. B. Giovenzana, *Org. Biomol. Chem.* **2014**, *12*, 6915–6921.
[22] J. Pfister, D. Summer, C. Rangger, M. Petrik, E. von Guggenberg, P. Minazzi, G. B. Giovenzana, L. Aloj, C. Decristoforo, *EJNMMI Res.* **2015**, *5*, 74.
[23] L. Greifenstein, T. Grus, J. Nagel, J. P. Sinnes, F. Rösch, *Appl. Radiat. Isot.* **2020**, *156*, 108867–108876.
[24] S. Ghiani, I. Hawala, D. Szikra, G. Trencsényi, Z. Baranyai, G. Nagy, A. Vágner, R. Stefania, S. Pandey, A. Maiocchi, *Eur. J. Nucl. Med. Mol. Imaging* **2021**, *48*, 2351–2362.
[25] A. L. Petersen, T. Binderup, R. I. Jølck, P. Rasmussen, J. R. Henriksen, A. K. Pfeifer, A. Kjær, T. L. Andresen, *J. Controlled Release* **2012**, *160*, 254–263.
[26] Z. Baranyai, S. Ghiani, A. Maiocchi, I. Hawala, WO2020099398 A1, **2020**.
[27] L. Manzoni, L. Belvisi, D. Arosio, M. P. Bartolomeo, A. Bianchi, C. Brioschi, F. Buonsanti, C. Cabella, C. Casagrande, M. Civera, M. De Matteo, L. Fugazza, L. Lattuada, F. Maisano, L. Miragoli, C. Neira, M. Pilkington-Miksa, C. Scolastico, *ChemMedChem* **2012**, *7*, 1084–1093.
[28] S. Pandey, G. B. Giovenzana, D. Szikra, Z. Baranyai, in *Metal Ions in Bio-Imaging Techniques* (Eds.: A. Sigel, E. Freisinger, R. K. O. Sigel), De Gruyter, Berlin, **2021**, pp. 315–346.
[29] É. Csajbók, Z. Baranyai, I. Bányai, E. Brücher, R. Király, A. Müller-Fahrnow, J. Platzek, B. Radüchel, M. Schäfer, *Inorg. Chem.* **2003**, *42*, 2342–2349.
[30] L. M. P. Lima, M. Beyler, R. Delgado, C. Platas-Iglesias, R. Tripier, *Inorg. Chem.* **2015**, *54*, 7045–7057.
[31] R. Pujales-Paradela, A. Rodríguez-Rodríguez, A. Gayoso-Padula, I. Brandariz, L. Valencia, D. Esteban-Gómez, C. Platas-Iglesias, *Dalton Trans.* **2018**, *47*, 13830–13842.
[32] V. I. Kornev, A. V. Trubachev, *Russ. J. Inorg. Chem.* **1987**, *32*, 2433–2437.
[33] M. W. Brechbiel, O. A. Gansow, C. G. Pippin, R. D. Rogers, R. P. Planalp, *Inorg. Chem.* **1996**, *35*, 6343–6348.
[34] Deposition Numbers 2115292 (for [Bi(HAAZTA)(H_2O)]·3H_2O) and 2115291 (for {[$C(NH_2)_3$][Bi(AAZTA)]}·3.5H_2O) contains the supplementary crystallographic data for this paper. These data are provided free of charge by the joint Cambridge Crystallographic Data Centre and Fachinformationszentrum Karlsruhe Access Structures service.
[35] S. Aime, G. Bombieri, C. Cavallotti, G. B. Giovenzana, D. Imperio, N. Marchini, *Inorg. Chim. Acta* **2008**, *361*, 1534–1541.
[36] G. Nagy, D. Szikra, G. Trencsenyi, A. Fekete, I. Garai, A. M. Giani, R. Negri, N. Masciocchi, A. Maiocchi, F. Uggeri, I. Toth, S. Aime, G. B. Giovenzana, Z. Baranyai, *Angew. Chem. Int. Ed.* **2017**, *56*, 2118–2122; *Angew. Chem.* **2017**, *129*, 2150–2154.
[37] Z. Baranyai, D. D. Castelli, C. Platas-Iglesias, D. Esteban-Gomez, A. Bényei, L. Tei, M. Botta, *Inorg. Chem. Front.* **2020**, *7*, 795–803.
[38] R. Fischer, J. Wendel, B. Dresow, V. Bechtold, H. C. Heinrich, *Appl. Radiat. Isot.* **1993**, *44*, 1467–1472.
[39] H. S. Chan, M. W. Konijnenberg, T. Daniels, M. Nysus, M. Makvandi, E. de Blois, W. A. Breeman, R. W. Atcher, M. de Jong, J. P. Norenberg, *EJNMMI Res.* **2016**, *6*, 83.

Manuscript received: May 14, 2022
Accepted manuscript online: September 8, 2022
Version of record online: September 29, 2022